Theory of third-harmonic generation using Bessel beams, and self-phase-matching

Surya P. Tewari,[1,2] H. Huang,[3] and R. W. Boyd[1]
[1]*Institute of Optics, University of Rochester, Rochester, New York 14627*
[2]*School of Physics, University of Hyderabad, Hyderabad Andhra Pradesh 500 046, India*
[3]*Department of Physics and Astronomy, University of Rochester, Rochester, New York 14627*
(Received 8 November 1995)

Taking Bessel beams (J_0 beam) as a representation of a conical beam, and a slowly varying envelope approximation (SVEA) we obtain the results for the theory of third-harmonic generation from an atomic medium. We demonstrate how the phenomenon of self-phase-matching is contained in the transverse-phase-matching integral of the theory. A method to calculate the transverse-phase-matching integral containing four Bessel functions is described which avoids the computer calculations of the Bessel functions. In order to consolidate the SVEA result an alternate method is used to obtain the exact result for the third-harmonic generation. The conditions are identified in which the exact result goes over to the result of the SVEA. The theory for multiple Bessel beams is also discussed which has been shown to be the source of the wide width of the efficiency curve of the third-harmonic generation observed in experiments. [S1050-2947(96)00308-3]

PACS number(s): 42.65.Ky, 32.80.Wr, 33.80.Wz

I. INTRODUCTION

Recently Glushko, Kryzhanovsky, and Sarkisyan have demonstrated [1] the phenomenon of self-phase-matching (SPM) for an efficient third-harmonic generation (THG) in atomic vapors. They employ a ring pump geometry. The ring slit[1] is illuminated by an expanded beam from a Nd:YAG laser. The emanating radiation, focused into a cell containing atomic vapors, generates a third harmonic (TH) which is observed at the end of the sample. The observed THG has been shown to be efficient compared to that due to a disclike source of the same power of the incident fundamental radiation. Besides this increase in efficiency the remarkable feature of the SPM lies in the large tolerance it accepts in the fluctuations of the refractive index mismatch between the fundamental and the TH. This mismatch may be due to the variation of pressure, temperature, or Kerr nonlinearity. The large tolerance in the refractive index also widens the frequency spread of the fundamental that can be used to give the TH. In short the concept of SPM has important implications.

In a rapid communication [2] we have reported a theory based on an idealized representation of the conical beam used in Ref. [1]. The theory explains salient features of the THG experiments of Ref. [1]. In this paper we give the details of this theory. We justify below the use of the Bessel beams in the theory; explain the slowly varying envelope approximation (SVEA) used to obtain the reported results in [2]; and further consolidate the SVEA results by deriving them by an alternate procedure. We then use the theory to consider THG using a double-conical beam, to demonstrate that the resulting TH is a superposition of four Bessel beams, and that a double-conical beams system can tolerate wider fluctuations in a refractive index compared to the beams produced by a single narrow ring slit or even a single broad ring slit. The case of representing a single broad ring slit by a series of ring slits placed side by side concentrically is discussed in detail using the approximate representation considered in the Appendix. The effects of reducing the radii of the ring slit and the focal length of the lens employed are considered at the end.

The use of Bessel beams is justified by two observations: (1) that the Bessel beam solution of the scalar wave equation is a superposition of infinite plane waves with their wave vectors parallel to the generators of a cone [3] representing an ideal conical beam; and note that it is such a superposition in which the authors of Ref. [1] analyze the concept of SPM; (2) that the method of generating the conical fundamental radiation using the ring slit in Ref. [1] is very similar to the method used by Durnin, Miceli, and Eberly [4] to demonstrate the realizability of the Bessel beam. Compare the similarities and the dissimilarities of the lens plus ring slit arrangement used in Ref. [1] and that used in Ref. [4] (also see the Appendix). In Ref. [1] the wider width ($\simeq$10 000 μm) of the ring slit and its nonplacement at the front focal plane of the lens may be noted. In Ref. [4] the ring slit is of narrower width ($\simeq$10 μm), and it is placed at the front focal plane of the lens. This ensured in Ref. [4] the plane-wave fronts in the image space for the field generated by a point on the ring slit. Thus the dissimilarities of the arrangements in [1] compared to that in [4] create curved-wave fronts in the focal region of the arrangement of [1], however the similarities suggest that the beams in [1] can—in first approximation—be taken to be a Bessel beam, or related to the Bessel beam of the type demonstrated by Durnin, Miceli, and Eberly [3,4].

The theoretical results presented in Ref. [2] on the basis of the J_0 beam show variations of the intensity of the generated TH, with the pressure of the atomic vapor, similar to the one observed in the experiments. The theory also shows the variation of the angular spread of the generated TH with pressure in that at low pressure the TH is widely spread,

[1]The ring slit used in Ref. [1] can be assumed to have a sharp inner radius and diffused outer radius determined by the falling Gaussian intensity of the expanded Nd:YAG beam.

coming all along the directions of the fundamental radiation. As pressure increases the angular spread narrows and the intensity increases. Finally at a critical value of the pressure the angular spread reduces only to a line along the symmetry axis. The intensity vanishes all together for pressures beyond it.

This paper is organized as follows. In Sec. II A we recapitulate some properties of Bessel beams, in II B we give the details of the slowly varying envelope treatment for the generation of the TH by a Bessel beam of the fundamental radiation. In Sec. II C it is demonstrated how the transverse-phase-matching is taken into account by the transverse-phase-matching integral (TPMI). A method to evaluate the TPMI is described.

Section III contains exact treatment not presented in [2] for a THG by a Bessel beam. The results of this section are valid, also, for the small sample length. In the limit of the long sample length, the expression of Sec. II is recovered.

Section IV discusses the multiple Bessel beam situation. We first describe the two-ring slit produced double-Bessel-beam configuration. The behavior of the cone angles of the resulting four Bessel beams is predicted. In Sec. IV B the case of three Bessel beams is briefly discussed, wherein one encounters as many as ten Bessel beams in the generated TH. Section IV C, discusses the case of a broad ring slit similar to the one used in Ref. [1]. It is found here that intensities of the generated TH are higher and the width of the tolerance in the variation of the refractive index is large. Lastly we discuss the results due to the variation of the ring-slit radii and the focal length of the lens used.

II. THE SLOWLY VARYING ENVELOPE FORMALISM FOR BESSEL BEAMS

Before we develop the slowly varying envelope formalism for the Bessel beams we recapitulate some properties of the Bessel beams [3–6].

A. The Bessel beam solution

Durnin [3] pointed out the existence of the circularly symmetric solution $\psi(\rho,z)$ involving the 0th order Bessel function, J_0,

$$\psi(\rho,z)=Ae^{-ik\,\cos(\alpha)z}J_0[k\,\sin(\alpha)\rho]e^{i\omega t}+\text{c.c.},$$
$$\rho^2=x^2+y^2, \tag{2.1}$$

of the scalar wave equation;

$$\nabla^2\psi-\frac{1}{c^2}\frac{\partial^2}{\partial t^2}\psi=\frac{4\pi}{c^2}\frac{\partial^2}{\partial t^2}P,$$
$$\nabla^2=\frac{\partial^2}{\partial x^2}+\frac{\partial^2}{\partial y^2}+\frac{\partial^2}{\partial z^2}, \tag{2.2}$$

and z is called the principal direction of propagation. For a linear medium one has

$$P=\chi^{(1)}(\omega)\psi, \tag{2.3}$$

$$k^2=\frac{\omega^2}{c^2}[1+4\pi\chi^{(1)}(\omega)]. \tag{2.4}$$

$\chi^{(1)}(\omega)$ is the linear susceptibility of the medium for light of the angular frequency ω. c is the velocity of light in vacuum. α in (2.1) is the angle of the cone which has its generators parallel to the infinity of infinite-plane waves that superpose to produce the solution (2.1) of (2.2). Thus

$$\psi(\rho,z)=Ae^{i\omega t}\int_0^{2\pi}e^{-ik\,\cos(\alpha)z-ik\,\sin(\alpha)\{x\,\cos(\phi)+y\,\sin(\phi)\}}\frac{d\phi}{2\pi}+\text{c.c.}, \tag{2.5}$$

(2.5) represents superposition of all plane waves with wave vectors $\vec{k}[=(k\,\sin(\alpha)\cos(\phi),\ k\,\sin(\alpha)\sin(\phi),\ k\,\cos(\alpha))]$. Thus all wave vectors have the same magnitude k and the same inclination α with the principal direction of propagation. The angle α can have arbitrary value in the range $0<\alpha<\pi$. One has the Bessel beam propagating along the positive z axis for $0<\alpha<\pi/2$ and along the negative z axis for $\pi/2<\alpha<\pi$. Note that (2.5) may also be written as

$$\psi(\rho z)=\frac{Ae^{i\omega t}}{2\pi k\,\sin\alpha}\int\exp(-ik_{\|}z-i\vec{k}_{\perp}\cdot\vec{\rho})\times\delta(k_{\|}-k\,\cos\alpha)\,\delta(k_{\perp}-k\,\sin\alpha)d^2k_{\perp}dk_{\|}+\text{c.c.},$$
$$k^2=k_{\|}^2+k_{\perp}^2,\quad d^2k_{\perp}=k_{\perp}dk_{\perp}d\phi. \tag{2.6}$$

(2.6) implies that for the Bessel beam one has superposition of waves of a fixed longitudinal wave vector $k_{\|}(=k\,\cos\alpha)$ and all possible directions of the transverse wave vector $k_{\perp}$ but with a fixed length $k_{\perp}=k\sin\alpha$. Here $(k_{\|},\ k_{\perp},\ \phi)$ are cylindrical coordinates in the k space.

Next we take the fundamental radiation in the form (2.1) and determine the amplitude of the generated third harmonic in the slowly varying envelope approximation.

B. THG using Bessel beam

In a nonlinear medium, the polarization oscillating at the frequency of the TH is given by

$$P_3=[\chi^{(1)}(\omega_3)\psi_3+\chi^{(3)}(\omega,\omega,\omega)\psi^3]. \tag{2.7}$$

Here, $\chi^{(1)}(\omega_3)$, and $\chi^{(3)}(\omega,\omega,\omega)$ are, respectively, the linear and the nonlinear susceptibilities at the frequency ω_3. The amplitude ψ_3 of the TH is determined by the scalar wave equation

$$\nabla^2\psi_3-\frac{1}{c^2}\frac{\partial^2}{\partial t^2}\psi_3=\frac{4\pi}{c^2}\frac{\partial^2}{\partial t^2}P_3. \tag{2.8}$$

Now, anticipating circular symmetry, (2.8) is written in cylindrical coordinates as

$$\left[\frac{\partial^2}{\partial\rho^2}+\frac{1}{\rho}\frac{\partial}{\partial\rho}+\frac{1}{\rho^2}\frac{\partial^2}{\partial\phi^2}+\frac{\partial^2}{\partial z^2}+\frac{\omega_3^2}{c^2}\right]\Psi_3^+ = -\frac{4\pi^2\omega_3^2}{c^2}P_3^+ = -\frac{4\pi^2\omega_3^2}{c^2}[\chi^{(1)}(\omega_3)\Psi_3^+ + \chi^{(3)}(\omega,\omega,\omega)\Psi^{+3}], \tag{2.9}$$

$$P_3 = P_3^+ e^{i3\omega t} + \text{c.c.}, \tag{2.10}$$

$$\psi_3 = \Psi_3^+ e^{i3\omega t} + \text{c.c.}, \tag{2.11}$$

$$\Psi^+ = Ae^{-ik\cos(\alpha)z}J_0(k\sin(\alpha)\rho), \tag{2.12}$$

$$\omega_3 = 3\omega. \tag{2.13}$$

For the sake of simplicity the susceptibilities dealing with other nonlinear responses of the medium are suppressed in (2.9)—assuming that they are small and noninterfering with the THG. It is also assumed that the THG has a negligible reaction on the fundamental wave, in that there is no wavefront distortion, and no depletion of the fundamental due to it. In this weak-coupling approximation the propagation of the fundamental in the medium is described by (2.2) and (2.3). Further, we assume the following factorized form for Ψ_3^+:

$$\Psi_3^+ = a(z)\exp(-ik_3\cos(\beta)z)J_0(k_3\sin(\beta)\rho). \tag{2.14}$$

Here, $a(z)$ is the slowly varying envelope of the generated Bessel beam of the TH. The angle β is to be determined from a condition to be discussed below.

On using: (i) the (2.14), in (2.9); (ii) the Bessel's equation for the zeroth order Bessel function in ρ; and dropping terms containing $[\partial^2 a(z)/\partial z^2]$ compared to those containing $k_3[\partial a(z)/\partial z]$ and $k_3^2 a(z)$, one obtains

$$2ik_3\cos(\beta)J_0(k_3\sin(\beta)\rho)\frac{\partial a(z)}{\partial z} = \frac{4\pi^2\omega_3^2}{c^2}\chi^{(3)}(\omega,\omega,\omega)\exp\{(ik_3\cos(\beta) - 3ik\cos(\alpha))z\}\{AJ_0(k\sin(\alpha)\rho)\}^3. \tag{2.15}$$

Now, multiplying both sides by $[k_3\rho\sin(\beta)J_0(k_3\sin(\beta)\rho)]$, and integrating over ρ $(0<\rho<\infty)$ yields

$$\frac{\partial a(z)}{\partial z} = \frac{2\pi\omega_3^2 A^3}{c^2 i}L\tan(\beta)\exp[i(k_3\cos(\beta)-3k\cos(\alpha))]z \times\chi^{(3)}(\omega,\omega,\omega)\int_0^\infty \rho J_0(k_3\sin(\beta)\rho) \times[J_0(k\sin(\alpha)\rho)]^3 d\rho. \tag{2.16}$$

Use has been made of Lommel's result [7] for an integral over the product of the two Bessel functions of zeroth order. Solving (2.16) for the amplitude of the generated third harmonic at the end face of a sample of length L gives

$$\Psi_3^+ = \exp -0.5iL[k_3\cos(\beta)+3k\cos(\alpha)]J_0(k_3\sin(\beta)\rho)2\pi \times\frac{\omega_3^2 A^3}{c^2 i}\tan(\beta)L\chi^{(3)}(\omega,\omega,\omega)\left(\frac{\sin(\theta)}{\theta}\right)\mathsf{I}, \tag{2.17}$$

$$\theta = 0.5L(k_3\cos(\beta)-3k\cos(\alpha)), \tag{2.18}$$

$$\mathsf{I} = 2\pi\int_0^\infty \rho J_0(k_3\sin(\beta)\rho)[J_0(k\sin(\alpha)\rho)]^3 d\rho \tag{2.19}$$

$$= \frac{1}{(k\sin\alpha)^2}\mathsf{F}(\mathsf{T}), \quad \mathsf{T} = \frac{k_3\sin(\beta)}{k\sin(\alpha)}. \tag{2.20}$$

(2.17) is the result quoted in Ref. [2][2]. It represents the solution of (2.8), as a Bessel beam of cone angle β. However the angle β still remains to be determined. Recall that for large sample lengths, i.e., for $L \gg \lambda/3$, the sync function $(\sin\theta/\theta)$ has appreciable value only in the range where,

$$k_3\cos(\beta) - 3k\cos(\alpha) = 0.0. \tag{2.21}$$

Thus for large interaction lengths the longitudinal phase-matching condition (2.21) determines the value of angle β. The behavior of the TPMI, $\mathsf{I}(\mathsf{T})$ is demonstrated in Fig. 1 of Ref. [2]. In brief, it is shown there that the amplitude of the Bessel beam of the generated third harmonic is maximum if the longitudinal phase-matching condition (2.21) and $\mathsf{T}=1$, is satisfied simultaneously. A discussion of the results is facilitated by characterizing the medium with an angle μ according to

$$\cos\mu = \frac{k_3}{3k} = 1 + \frac{\Delta\chi(\omega_3,\omega)}{[1+2\pi\chi^{(1)}(\omega)][1+2\pi\chi^{(1)}(\omega_3)]}, \tag{2.22}$$

$$\Delta\chi(\omega_3,\omega) = 2\pi[\chi^{(1)}(\omega_3) - \chi^{(1)}(\omega)]. \tag{2.23}$$

The angle μ defined by (2.22), can be modified by a variation of pressure and temperature, as it is dependent on the linear susceptibilities of the medium. The transverse ratio T also depends on the medium properties through the angle μ and on the geometry through the angle α of the fundamental Bessel beam. Note, that for the negatively dispersive media both the angles the μ and the β (from Eq. (10) of Ref. [2]), are to be equal to or less than the cone angle α of the fundamental Bessel beam.

For a positively dispersive medium, definition of the angle μ by the use of Eq. (2.22) is improper as $k_3 > 3k$. In this case the condition for longitudinal phase matching can still be satisfied by choosing $\beta > \alpha$. However the transverse-phase-matching factor is then

[2]The K_3 in the denominator of the prefactor in Eq. (5) of Ref. [2] is to be replaced by length L in the numerator as in (2.17) above. The additional phase factor in (2.17) does not contribute to the intensity of THG. It is made explicit here to demonstrate the equivalence of (2.17) to (3.19) derived later in the paper.

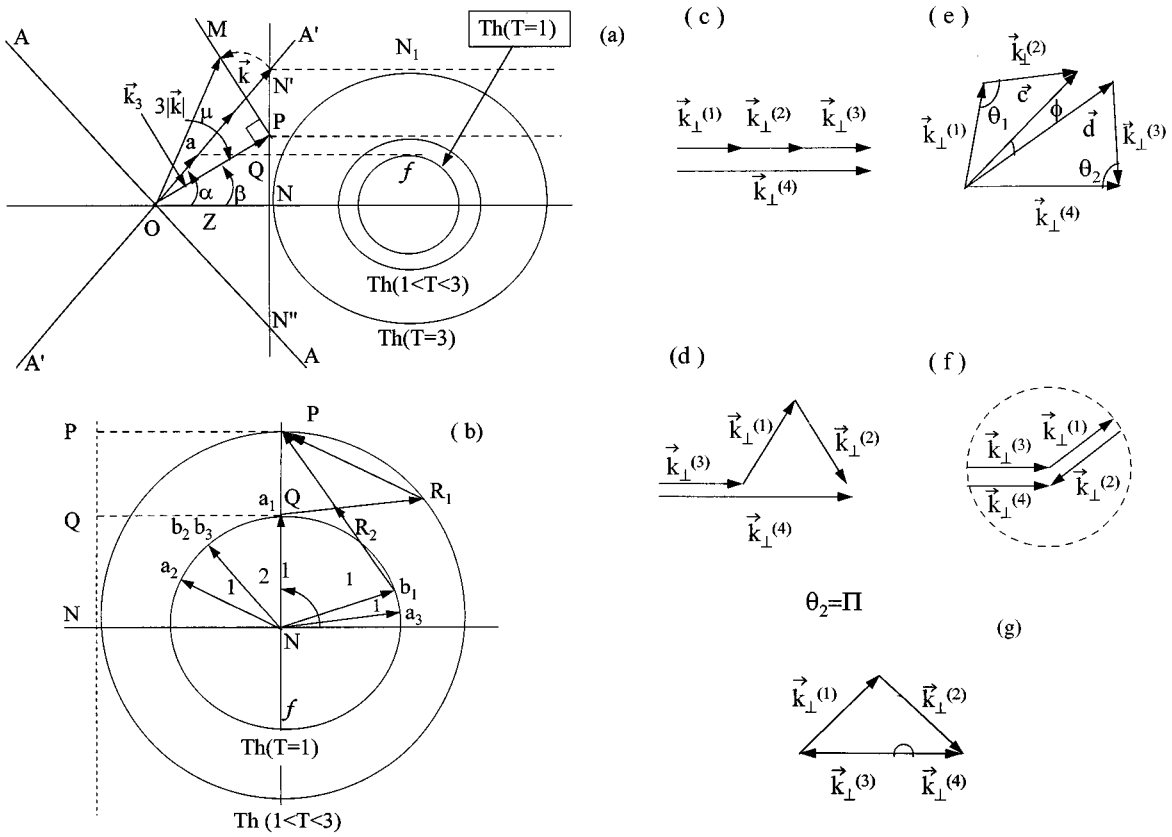

FIG. 1. (a) The sections of the cones of the fundamental, and the third-harmonic wave vectors are shown; (b) the details of the positions of the transverse components for transverse-phase matching discussed in the text are shown; (c)–(g) show examples of transverse-phase-matching quadrilaterals for some chosen cases (see text); diagram (e) is relevant for the evaluation of TPMI. The lengths of some vectors are not exactly to the same scale as implied in the text. This defect may be ignored.

$$\mathsf{T}=3\left\{1+\left[\left(\frac{k_3}{3k}\right)^2-1\right]\frac{1}{\sin^2\alpha}\right\}^{1/2}, \tag{2.24}$$

$$>3 \quad \forall\alpha. \tag{2.25}$$

We know that the TPMI vanishes for $\mathsf{T}>3$. Thus positively dispersive media do not support self-phase-matching.

Equation (2.17), quoted in [2] is the main result of the Bessel beam representation of the conical beam. It demonstrates linear dependence on the length L of the medium provided the phase matching is satisfied. In contrast to the plane-wave situation the phase matching is broken into two parts. The longitudinal part is represented by the sync function, and the transverse part is contained in TPMI. We elaborate next on the TPMI.

C. The transverse-phase-matching integral

Before we discuss the calculations of the phase-matching integral it is instructive to show how it takes into account the different possibilities of the SPM. Consider the graphic representation in Fig. 1 of various parameters defined here and in Ref. [2].

Two sections of the cones of the wave vectors of the fundamental ($\vec{k}$) and the generated third-harmonic ($\vec{k}_3$) are represented in Fig. 1(a). The left side of line $N'N''$ shows the longitudinal section cut by a plane containing the principal axis OZ of the cones. The right side of the line $N'N''$ in Fig. 1(a) shows the transverse section (or the side view) of the cones as seen on a plane perpendicularly to the principal axis OZ at N, and parallel to the line $N'NN''$. In the longitudinal section AA, $A'A'$ are along the generators of the cone of the fundamental, and OP is along the generator of the cone of the third harmonic. The angle α (β) is the angle of the cone of the fundamental (TH). As the pressure of the gas is increased the point P ($OP=|\vec{k}_3|$) in Fig. 1(a) moves along $N'PN$ and β changes from $\beta=\alpha$, to $\beta=0$, all the time maintaining the longitudinal phase-matching condition (2.21). Note that the length $l_{ON'}=|3\vec{k}|$. The angle μ characterizing the medium is also depicted by the right-angled triangle OMP, such that $l_{OM}=l_{ON'}$. At $\mu=0$, the points M, N', P coincide at N'; and at $\mu=\alpha$ coincidence takes the place of M with N', and of P with N. In the transverse section the circle marked TH (f) is the locus of the tip of the third-harmonic wave vector $\vec{k}_3$ along OP (fundamental wave-vector $\vec{k}$ along Oa). Each TH circle is marked by the value of the corresponding ratio $\mathsf{T}=(k_3\sin\beta/k\sin\alpha)$. The f circle and the TH circle coincide for $\mathsf{T}=1$. For the sake of clarity no TH circle for $\mathsf{T}<1$ lying inside the f circle has been shown.

The different possibilities of transverse-phase matching which contribute to the TPMI, can be understood with reference to Figs. 1(a)–1(g) which give the details of the positions and directions of the transverse components of the wave vectors of the fundamental and the TH. First, note that,

in Figs. 1(a) and 1(b), the radial vectors (like $\vec{v}_{NQ}$ defined by the direction pointing from N to Q, and by a magnitude equal to the line segment NQ) of the f circle, represent all possible directions of the transverse vector $k_\perp = |k \sin\alpha|\hat{n} = |k \sin\alpha|(\cos\Gamma, \sin\Gamma)$ where Γ is the angle with any arbitrarily chosen x axis in the transverse plane. The radial vectors, $\vec{v}_{NP}$, of the TH circle, similarly, represent the transverse vectors $k_3^{(T)} = \vec{k}_\perp^{(4)}$ of the TH (see below and Figs. 1(c)–1(g) for notation).

Now, consider in Fig. 1(a) the $\mathsf{T}=3$ at $\mu=0$ case, when the point P lies on N'. Recall that $\beta=\alpha$ for $\mu=0$. The transverse-phase matching, in this case, is represented by the vectorial equation along NN' [see Fig. 1(c)]

$$\vec{k}_\perp^{(4)} = \vec{v}_{NN'} = 3\vec{v}_{NQ} = \vec{k}_\perp^{(1)} + \vec{k}_\perp^{(2)} + \vec{k}_\perp^{(3)}. \tag{2.26}$$

A similar equation exists for each point on the TH-circle ($\mathsf{T}=3$), [Fig. 1(a)] implying that for collinear-phase matching the generated TH is emitted along each plane-wave component of the fundamental Bessel beam. Note that there is only one phase-matching diagram for each point of the TH-circle ($\mathsf{T}=3$).

Consider now, in Fig. 1(b), the TH-circle ($1<\mathsf{T}<3$) for which $k_\perp^{(4)} = \vec{v}_{NP}$. Here, we represent two of the several cases in which the transverse-phase matching can be achieved. The first case, is depicted by the set of vectors $\vec{v}_{Na_1} = \vec{k}_\perp^{(3)}$, $\vec{v}_{Na_2} = \vec{k}_\perp^{(1)}$ and $\vec{v}_{Na_3} = \vec{k}_\perp^{(2)}$. The planar quadrilateral which is implied by the transverse-phase matching condition is Na_1R_1P. The two sides viz. Na_1 and NP of the quadrilateral overlap and correspond to the case $\theta_2=0$ for the vectors, $\vec{k}_\perp^{(4)}$ and $\vec{k}_\perp^{(3)}$ of Fig. 1(d). The sides a_1R_1 and R_1P are provided by the radial vectors $\vec{v}_{Na_3}$ and $\vec{v}_{Na_2}$ of the f circle and therefore by the wave vectors available in the corresponding directions in the Bessel beam. The second case is depicted by the set of vectors $\vec{v}_{Nb_1} = \vec{k}_\perp^{(3)}$, $\vec{v}_{Nb_2} = \vec{k}_\perp^{(1)} = \vec{v}_{Nb_3} = \vec{k}_\perp^{(2)}$. The quadrilateral representing the transverse-phase matching is now seen to be Nb_1R_2P. The sides b_1R_2 and R_2P are provided by the parallel vectors $\vec{v}_{Nb_2}$. Note that the second case corresponds to the angle $\theta_2 = \theta_2^{\max}$ between the $\vec{k}_\perp^{(4)}$ and $\vec{k}_\perp^{(3)}$ [consider, for example, the $\theta_2^{\max}$ case, with $\phi=0$ and $\vec{c}=\vec{d}$ in Fig. 1(e)]. All values of θ_2 such that $0<\theta_2<\theta_2^{\max}$ are represented by the position of the radial vector $\vec{v}_{Nb_1}(\theta_2)$ lying between $\vec{v}_{Na_1}$ and $\vec{v}_{Nb_1}(\theta_2^{\max})$. It is not demonstrated in the diagram but it can be stated that the corresponding quadrilateral for each value of θ_2 such that $0<\theta_2<\theta_2^{\max}$ is always possible by taking two vectors viz. $\vec{v}_{Nb_2}$ and $\vec{v}_{Nb_3}$, not parallel to one another, to complete the quadrilateral Nb_1R_2P. Note that unlike the collinear-phase-matching case [which has only one diagram, Fig. 1(c)] one has contribution to the TPMI from all the diagrams of transverse-phase matching characterized by $0<\theta_2<\theta_2^{\max}$ for a $NP = k_3\sin\beta$. By symmetry, equal contribution also comes from diagrams with $(2\pi-\theta_2^{\max})<\theta_2<2\pi$. Thus the phase-matching integral of the present formalism takes into account all possible transverse-phase matchings. This is very different from the formalism adopted in Ref. [1]. For example it is not clear from Eq. (7) of Ref. [1] as to how these different cases are to be taken into account.

A picture similar to Fig. 1 can be drawn for $k_3>3k$. The point P will then lie above the point N' on the line NN' to make $\beta>\alpha$. The impossibility of meeting the transverse-phase-matching condition is noted by the fact that then $NP>NN'$ and that it cannot be made up by any vectorial sum of three vectors each of length $k \sin\alpha$ which total only up to a maximum of length $l_{NN'}$.

Next consider the evaluation of the TPMI I in (2.19) which can be written as

$$\mathsf{I} = \frac{1}{(2\pi)^4}\int_{-\infty}^{\infty}dx\int_{-\infty}^{\infty}dy\int_0^{2\pi}d\Gamma_1\int_0^{2\pi}d\Gamma_2 \times\int_0^{2\pi}d\Gamma_3\int_0^{2\pi}d\Gamma_4 \exp[i(\vec{k}_\perp^{(1)}+\vec{k}_\perp^{(2)}+\vec{k}_\perp^{(3)}+\vec{k}_\perp^{(4)})\vec{\rho}], \tag{2.27}$$

$$\vec{\rho} = \vec{i}x + \vec{j}y.$$

In going from (2.19) to (2.27), the circular symmetry and a representation of the Bessel function has been used. The $\vec{k}_\perp^{(i)}$, $i=1,2,3,4$ in (2.27), are the four, two-dimensional vectors, which are projections on the x-y plane [see Fig. 1(b)] of the four wave vectors viz. the three k vectors of the fundamental, and the fourth vector is the $\vec{k}_3$ of the generated TH. The Γ_i is the angle, in the x-y plane, between the two-dimensional vectors $\vec{\rho}$ and the $\vec{k}_\perp^{(i)}$. Note that the vectors $\vec{k}_\perp^{(i)}$ ($i=1,2,3$) have equal magnitude but arbitrary directions in the x-y plane. As long as the longitudinal phase matching is not imposed-$\vec{k}_\perp^{(4)}$ is also arbitrary in direction and length.

In order to estimate (2.27), divide the four planar vectors into two groups as shown in Fig. 1(e)

$$\vec{c} = \vec{k}_\perp^{(1)} + \vec{k}_\perp^{(2)}, \tag{2.28}$$

$$\vec{d} = \vec{k}_\perp^{(4)} - \vec{k}_\perp^{(3)}. \tag{2.29}$$

Let x and y axes be, respectively, along the vector $\vec{d}$ and perpendicular to the vector d. The integrations over the four angles Γ_i can now be performed by redefining $\Gamma_1=\theta_1$ to be the angle between $\vec{k}_\perp^{(1)}$ and $\vec{k}_\perp^{(2)}$; $\Gamma_2=\theta_2$ to be the angle between $\vec{k}_\perp^{(4)}$ and $\vec{k}_\perp^{(3)}$; $\Gamma_3=\theta_3=\phi$, to be the angle between the vector $\vec{c}$ and $\vec{d}$. The angle $\Gamma_4=\theta_4$ can be represented by the rotation of $\vec{c}$ and $\vec{d}$ vector system (intact) with respect to any arbitrary direction in the x-y plane. Since this last rotation produces similar systems, an integration over the θ_4 angle is readily performed, which yields the value 2π. Also performing the integrations for the x coordinate and the y coordinate there results two δ functions due to the infinite extension of the medium in the two directions. Thus

$$\mathsf{I} = \frac{1}{(2\pi)^3}\int d\theta_1\int d\theta_2\int d\phi\, 2\pi \times\delta[c\cos(\phi)-d]\,2\pi\,\delta[c\sin(\phi)], \tag{2.30}$$

$$c = 2k\sin(\alpha)\sin(0.5\theta_1), \tag{2.31}$$

$$d^2 = (k_3\sin(\beta))^2 + (k\sin(\alpha))^2 - 2k_3k\sin(\alpha)\sin(\beta)\cos\theta_2. \tag{2.32}$$

Now performing the integration over the angle ϕ using the second δ function, gives

$$\mathsf{I}=\frac{1}{2\pi}\int d\theta_1\int d\theta_2\,\delta(c-d)c^{-1}. \tag{2.33}$$

Finally using the remaining δ function to perform the integration over the angle θ_1, contained in the length of the vector c one gets

$$\mathsf{I}=\frac{1}{2\pi}\int_0^{2\pi} d\theta_2[(2k\,\sin(\alpha)\sin(0.5\theta_1)\times k\,\sin(\alpha)\cos(0.5\theta_1)]^{-1}. \tag{2.34}$$

Since, $d=c=2k\,\sin(\alpha)\sin(0.5\theta_1)$

$$\mathsf{I}=\frac{1}{\pi}\int_0^{\pi}\frac{1}{d\sqrt{(k\,\sin\alpha)^2-0.25d^2}}\,d\theta_2. \tag{2.35}$$

In the last step, use has been made of the equal contributions from 0 to π, and from π to 2π. Note that, one has to be careful with the upper limit of the integral in (2.35). The upper limit is π, for $T\leqslant 1$, e.g., Fig. 1(f) for $T=1$, and Fig. 1(g) as a representative case for $T<1$. For, $T>1$, the upper limit is $\theta_2=\theta_2^{\max}$, see in Fig. 1(b) the quadrilateral Nb_1R_2P. $\theta_2^{\max}$ may be determined by the condition that the pojection of $\vec{k}_\perp^{(1)}$ and $\vec{k}_\perp^{(2)}$ perpendicular to $\vec{d}$ becomes zero. This projection is exactly the term under the square root in (2.35). Thus at $\theta_2=\theta_2^{\max}$

$$4(k\,\sin\alpha)^2-d^2(\theta_2=\theta_2^{\max})=0.$$

The integrand in (2.35) gives a large contribution at $\theta_2=0$ for $0<T<3$. It develops another region which gives a large contribution to the integral at

$$\text{(i)}\quad \theta_2=\pi \quad \text{for } (\sqrt{2}-1)\leqslant T<1$$

$$\text{(ii)}\quad \theta_2=\theta_2^{\max} \quad \text{with } \cos(\theta_2^{\max})=[(T^2-3)/2T]$$

$$\text{for } 1<T\leqslant 3.$$

Note also that at $T=1$, (2.35) is a divergent integral, which essentially stems due to the infinite extension of the Bessel beam in the transverse directions. The overlap is thus maximum at $T=1$. The divergence at $T=1$ need not be disturbing, as such divergence is seen in Lommel's formula too. Lommel's formula and the integral (2.19) represent, respectively, the effective transverse areas over which the product of the Bessel beam with itself and of the cube of the fundamental with the generated third harmonic, have a nonzero value. The transverse-phase-matching diagram for $T=1$ is depicted in Fig. 1(f). Note that, because of the degeneracy in length, each point of the TH circle gets a contribution from every other point of the f circle. Figure 1 of Ref. [2] has been obtained from (2.35) by using different values of its parameters.

It will be helpful here to recapitulate the results of Ref. [1] along with those of the above expressions. The self-phase-matching case of $\beta\cong\alpha/3$, for small inclination α of Ref. [1] corresponds to the divergence at $T=1$ in the present formalism. Similarly their collinear-phase-matching case, where $\beta\cong\alpha$ corresponds here to the divergence at $T\cong 3$. The two divergences correspond to the diagrams 1(f) and 1(c) in Fig. 1, which demonstrates the ways the transverse-phase-matching condition is satisfied in these two cases. The $\beta=0$ case of [1] is obtained when the value of μ reaches its cutoff value α. We will use the result (2.17) in Sec. IV. In the following section we are concerned with the derivation of (2.17) from an expression which is valid beyond the slowly varying envelope approximation used in Sec. II B.

III. AN EXACT TREATMENT OF THE THIRD-HARMONIC GENERATION BY BESSEL BEAM

We consider the semi-infinite half-space ($0<\rho<\infty$, $0<z<\infty$) containing the nonlinear medium, and as in Sec. II, work within the scalar wave equation. Taking as usual the refractive index for the third-harmonic wave to be n_3, and (2.10–2.13) the (2.8) gives

$$\nabla^2\Psi_3^+ + n_3^2\frac{\omega_3^2}{c^2}\Psi_3^+ = -\mathcal{P}\psi^{+3}, \tag{3.1}$$

$$n_3^2=[1+4\pi\chi^{(1)}(\omega_3)], \tag{3.2}$$

$$\mathcal{P}=\frac{4\pi\omega_3^2\chi^{(3)}(\omega,\omega,\omega)}{c^2}. \tag{3.3}$$

In order to solve (3.1) consider the Fourier transform of both sides. We take

$$\Psi_3^+(\vec{X})=\int\hat{\Psi}_3(\vec{K})e^{-i\vec{K}\cdot\vec{X}}d\vec{K}, \tag{3.4}$$

$$\Psi^{+3}(\vec{X})=\frac{1}{(2\pi)^3}\int g(\vec{K})e^{-i\vec{K}\cdot\vec{X}}d\vec{K}, \tag{3.5}$$

where

$$g(\vec{K})=\int e^{i\vec{K}\cdot\vec{X}}\Psi^{+3}(\vec{X})d\vec{X}. \tag{3.6}$$

The $\hat{\Psi}_3(\vec{K})$ is determined from the algebraic relation in the $\vec{K}$ space. We get

$$\hat{\Psi}_3(\vec{K})=\frac{\mathcal{P}g(\vec{K})}{(2\pi)^3(K^2-k_3^2)},\quad k_3^2c^2=n_3^2\omega_3^2. \tag{3.7}$$

For the circularly symmetric ψ^+, one can write

$$g(\vec{K})=\int_{-\infty}^{+\infty}dz\;e^{i(\vec{K}_\parallel-3\vec{k}_\parallel)z}\int_0^\infty 2\pi\rho\,d\rho[J_0(k_\perp\rho)]^3J_0(K_\perp\rho), \tag{3.8}$$

$$=\frac{2\pi\delta(\vec{K}_\parallel-3\vec{k}_\parallel)}{(k_\perp)^2}\,\mathsf{F}(\mathfrak{R}), \tag{3.9}$$

$$\mathsf{F}(\mathfrak{R})=\int_0^\infty 2\pi\overline{\rho}\,d\overline{\rho}[J_0(\overline{\rho})]^3J_0(\mathfrak{R}\overline{\rho}), \tag{3.10}$$

$$\overline{\rho}=k_\perp\rho,\quad \mathfrak{R}=\frac{K_\perp}{k_\perp}. \tag{3.11}$$

Thus

$$\hat{\Psi}_3(\vec{K}) = \frac{\mathcal{P}\delta(K_\parallel - 3k_\parallel)}{(2\pi)^3 (k_\perp)^2} \frac{\mathsf{F}(\mathfrak{R})}{K^2 - k_3^2}. \tag{3.12}$$

(3.12) gives the amplitude of the forced wave in the nonlinear medium for the mode $\vec{K}$. The amplitude exists for all modes for which $g(K)$ is nonzero. Thus the amplitude (3.12) exist in the region of space $0 < z < L$ in which the medium pervades. The corresponding amplitude is determined from (3.4). However, the amplitude of only such modes is expected to grow, whose mode parameter $\vec{K}$ lies on the energy shell $K^2 = k_3^2$. For such modes (3.12) has singularity. A convenient way to take account of the singularity is to convert (3.12) into 0/0 form by adding the solution of the homogeneous part of (3.1), which exists only on the energy shell. The modified expression for the amplitude in K space, valid for all mode parameter $\vec{K}$, and that which satisfies the boundary condition in the ordinary space

$$\Psi_3(\vec{X})|_{z=0} = 0 \tag{3.13}$$

is given by

$$\hat{\Psi}_3(\vec{K}) = \frac{\mathcal{P}\mathsf{F}(\mathfrak{R})}{(2\pi)^3 (k_\perp)^2} \left[\frac{\delta(K_\parallel - 3k_\parallel) - \delta(K - k_3)}{K^2 - k_3^2} \right]. \tag{3.14}$$

The corresponding spatial amplitude is obtained by using (3.14) in (3.4). Taking advantage of the circular symmetry, the result can be written as

$$\Psi_3^+(\vec{X}) = \frac{\mathcal{P}A^3}{(2\pi)^2 (k_\perp)^2} \int_0^\infty K_\perp dK_\perp \mathsf{F}(\mathfrak{R}) J_0(K_\perp \rho) \left[\frac{2\pi\delta(K_\parallel - 3k_\parallel) e^{-iK_\parallel z} - 2\pi\delta(K - k_3) e^{-iz(k_3^2 - K_\perp^2)^{1/2}}}{[K_\perp^2 - (k_3^3 - K_\parallel^2)]} \right]. \tag{3.15}$$

While writing (3.15) use has been made in replacing $K_\parallel$ according to the two δ functions. The first term in the numerator in the square bracket admits all values of $K_\perp$, irrespective of the fact that the corresponding mode will or will not be supported by the medium. The second term on the other hand does the same but for $K_\parallel^2 = k_3^2 - K_\perp^2$. The combination of the two terms in (3.15) acts in such a way that at large distances only such forced modes will grow which are supported by the free wave solution. This may be demonstrated by the following modification of the square bracket; we may write the square bracket as

$$2\pi \left[\frac{e^{-3ik_\parallel z} - e^{-iz(k_3^2 - K_\perp^2)^{1/2}}}{i([k_3^2 - K_\perp^2]^{1/2} - 3k_\parallel)} \right] \frac{1}{\left[\dfrac{K_\parallel^2 - (k_3^2 - K_\perp^2)}{i([k_3^2 - K_\perp^2]^{1/2} - 3k_\parallel)} \right]}. \tag{3.16}$$

So in the limit of large z and $K^2 \to k_3^2$ (3.16) implies in addition to a phase factor the following expression:

$$(2\pi)^2 z[\text{unity if } (k_3^2 - K_\perp^2)^{1/2} \to 3k_\parallel] \frac{1}{[2iK_\parallel]}, \tag{3.17}$$

which could also mean to imply

$$K_\perp \to (k_3^2 - K_\parallel^2)^{1/2}, \quad \text{and } K_\parallel \to 3k_\parallel. \tag{3.18}$$

Making use of these expressions for large z, (3.15) can be simplified. It gives, along with the phase factor mentioned above, the result

$$\Psi_3^+(X) = \mathcal{P}A^3 \frac{K_\perp}{k_\perp^2 (2iK_\parallel)} z e^{-iK_\parallel z} J_0(K_\perp \rho) \mathsf{F}(\mathfrak{R}). \tag{3.19}$$

Now, if one takes

$$K_\parallel = k_3 \cos(\beta); \quad K_\perp = k_3 \sin(\beta); \quad k_\perp = k \sin(\alpha); \quad z = L \tag{3.20}$$

(3.19) becomes identical to the slowly varying envelope approximation result (2.17). The expression (3.16), however, is valid for all lengths of the sample. It is readily checked that the experiments of Ref. [1] can be analyzed using the slowly varying envelope result (2.17) of Sec. II or (3.19) above.

In the next section we use (2.17) to discuss the THG by the multiple Bessel beam incident fundamental.

IV. MULTIPLE BESSEL BEAMS

The numerical results of (2.17) for a model system giving a single Bessel beam, are discussed in Ref. [2]. The model chosen has the ring slit with radius $a = 0.45$ cm and the width $da = 0.1$ mm, the focal length of the convex lens is assumed to be 10.0 cm and $\lambda_3 = 0.355$ μ. The Bessel beam emerging from such a model system is derived in the Appendix. We use (A8) to represent the input Bessel beam. Figure 2 of Ref. [2] shows the total detected power ($|E_3|^2$) of the third harmonic as a function of pressure (proportional to $\{1 - \cos\mu\}$) normalized suitably. The detected power ($|E_3|^2$) is calculated using (2.17) according to

$$|E_3|^2 = 2\pi \int_0^a \rho \, d\rho |\Psi_3^+|^2.$$

It is assumed to be falling on a circular detector placed centrally and perpendicularly to the z axis at the end of the sample. The radius of the detector is $a > k_3 \sin(\alpha)$, where $\beta = \alpha$ is the largest cone angle which the generated Bessel beam of the third harmonic can have at collinear-phase-matching conditions ($\mu = 0.0$), which occurs at very low pressures (because in the vacuum there is no difference in the velocities of the fundamental and the third-harmonic waves). At low pressures there are fewer atoms in the cell, which

TABLE I. Single Bessel beam.

Medium angle μ	Transverse ratio T	Output angle β	Phase-Matching integral I	Nature of Phase-Matching CP/SP
0	3	α	$\neq 0$	Collinear-Phase Matching
α	0	0	$\neq 0$	Self-Phase Matching
μ_0	1	β_0	maximum	Self-Phase Matching

produce small amplitudes of the generated third-harmonic wave. As the pressure is increased the phase mismatch $\Delta\chi(\omega_3,\omega)$ becomes significant, the collinear-phase matching can no longer be satisfied. It is in this domain that the advantages due to the possibilities of self-phase matching set in. Simultaneous satisfaction of the longitudinal and the transverse-phase matching becomes possible—and the amount of the third harmonic generated depends on the effective area over which there is significant overlap of the transverse variations of the cube of the fundamental and the third-harmonic Bessel beam. The maximum occurs at $k_3\sin(\beta)=k\sin(\alpha)$ at which

$$\tan(\beta_0)=(1/3)\tan(\alpha).$$

On further increase of the pressure the effective area decreases but does not vanish. The decrease is controlled by the $\tan(\beta)$ and by the sharp cutoff at $\mu>\alpha$ when $I=0$.

The values of the parameters T,β,I along with the nature of phase matching occurring at different values of the medium angle μ for a single Bessel beam are summarized in Table I, for ready reference.

We consider now how by having more than one Bessel beam in the input radiation one can have a broader width like that shown in Fig. (3) of Ref. [2].

A. Third-harmonic generation using two Bessel beams

Consider two thin-ring slits of radii a_1 and a_2 $(a_1<a_2)$. Their widths da_1 and da_2 are very small compared to their radii. The two radii can be arbitrarily close to one another. For definiteness, let these two ring slits generate distinct Bessel beams, of cone angles α_1 and α_2, $(\alpha_1<\alpha_2)$, respectively. These Bessel beams overlap in the nonlinear medium generating the third harmonic. The fundamental field in the medium is represented by

$$\Psi_1^+=e^{i\omega t}[A_1e^{-ik\cos(\alpha_1)z}J_0(k\sin(\alpha_1)\rho) + A_2e^{-ik\cos(\alpha_2)z}J_0(k\sin(\alpha_2)\rho)], \tag{4.1}$$

A_1 and A_2 are the amplitudes of the two Bessel beams. These are determined, as discussed briefly in the Appendix, by the field illuminating the ring slits, and the widths of the ring slits. The generated third-harmonic amplitude in the long-sample limit is given by

$$\Psi_3^+=\frac{2\pi\omega_3^2}{ic^2}\chi^{(3)}(\omega,\omega,\omega)\xi(z), \tag{4.2}$$

$$\xi(z)=z[2\pi A_1^3I_1\Xi(\beta)\delta(y_1)+2\pi 3A_1^2A_2I_2\Xi(\beta)\delta(y_2) + 2\pi 3A_1A_2^2I_3\Xi(\beta)\delta(y_3)+2\pi A_2^3I_4\Xi(\beta)\delta(y_4)], \tag{4.3}$$

$$\Xi(\beta)=\tan(\beta)J_0(k_3\sin(\beta)\rho)e^{-ik_3\cos(\beta)z},$$
$$y_1=k_3\cos(\beta)-3k\cos(\alpha_1),$$
$$y_2=k_3\cos(\beta)-2k\cos(\alpha_1)-k\cos(\alpha_2),$$
$$y_3=k_3\cos(\beta)-k\cos(\alpha_1)-2k\cos(\alpha_2),$$
$$y_4=k_3\cos(\beta)-3k\cos(\alpha_2), \tag{4.4}$$

$$I_1=\int_0 2\pi\rho\,d\rho\;J_0^3(k\sin(\alpha_1)\rho)J_0(k_3\sin(\beta)\rho), \tag{4.5a}$$

$$I_2=\int_0^\infty 2\pi\rho\,d\rho\;J_0^2(k\sin(\alpha_1)\rho) \times J_0(k\sin(\alpha_2)\rho)J_0(k_3\sin(\beta)\rho), \tag{4.5b}$$

$$I_3=\int_0^\infty 2\pi\rho\,d\rho\;J_0(k\sin(\alpha_1)\rho) \times J_0^2(k\sin(\alpha_2)\rho)J_0(k_3\sin(\beta)\rho), \tag{4.5c}$$

$$I_4=\int_0^\infty 2\pi\rho\,d\rho\;J_0^3(k\sin(\alpha_2)\rho)J_0(k_3\sin(\beta)\rho). \tag{4.5d}$$

It is clear from the above that a photon of the generated third harmonic can come from four different combinations of the three photons of the fundamental beams: (1) all three photons come from the α_1 beam; (2) all three photons come from the α_2 beam; (3) one photon comes from the α_2 beam and two photons come from the α_1 beam; and (4) two photons come from α_2 beam and one photon comes from the α_1 beam. Consequently there are four different longitudinal phase-matching conditions represented by the four δ functions in (4.3). Thus the generated third-harmonic field can be in a superposition of four distinct Bessel beams, their angles being determined by the prevailing conditions in the sample. In order to develop a scheme to label the four distinct beams, recall that for the single thin-ring-slit case, a Bessel beam is produced when

$$0 \leqslant \mu \leqslant \alpha. \tag{4.6}$$

From (4.6) and from Table I it is seen that the output radiation has a separate Bessel beam for each input Bessel beam corresponding to the angles α_1 and α_2. In addition there are two other angles $\alpha^{(3)}$ and $\alpha^{(4)}$ defined by

$$3\cos(\alpha^{(3)}) = 2\cos(\alpha_1) + \cos(\alpha_2), \tag{4.7}$$

$$3\cos(\alpha^{(4)}) = \cos(\alpha_1) + 2\cos(\alpha_2), \tag{4.8}$$

which determine the additional two Bessel beams in the output radiation. The cone angles β_1, β_2, β_3, and β_4 of the four Bessel beams which constitute the output radiation are determined from the respective longitudinal phase-matching conditions, and are given by

$$\begin{aligned} \cos(\beta_1) &= \frac{\cos(\alpha_1)}{\cos\mu}, \\ \cos(\beta_2) &= \frac{\cos(\alpha^{(3)})}{\cos\mu}, \\ \cos(\beta_3) &= \frac{\cos(\alpha^{(4)})}{\cos\mu}, \\ \cos(\beta_4) &= \frac{\cos(\alpha_2)}{\cos\mu}. \end{aligned} \tag{4.9}$$

Using the eight angles, one has the following possibilities between the input and output Bessel beams in the case of the two thin-ring slits:
(a) four Bessel beams, with β_1, β_2, β_3 and β_4 for $0<\mu<\alpha_1$;
(b) three Bessel beams with angles β_2, β_3, β_4 for $\alpha_1<\mu<\alpha^{(3)}$;
(c) two Bessel beams with angles β_2, β_4 for $\alpha^{(3)}<\mu<\alpha^{(4)}$;
(d) one Bessel beam with angle β_2 for $\alpha^{(4)}<\mu<\alpha_2$; and
(e) no Bessel beam for $\alpha_2<\mu$.

The amplitude of each Bessel beam component in the output is determined by the corresponding TPMI viz. I_1, I_2, I_3, I_4. Figure 2 shows the behaviors of I_1, I_2, I_3, and I_4 for the model system $a_1=0.45$ cm, $a_2=0.55$ cm, $da_1=da_2=0.01$ cm, $f=10.0$ cm, and for various values of the pressures. The double peaks in I_2 and I_3 are easily understood to be the two alternate ways the overlap integral can acquire a local maximum.

Figure 3 demonstrates the intensity of the generated TH recorded by the detector placed at $z=10.0$ cm. The curves *a* and *b* correspond to the situations when either α_1 or α_2 input Bessel beam is only present. The curve *c* represents the generation of the third harmonic when the α_1 and α_2 Bessel beams are simultaneously present in the sample. This Fig. 3 clearly demonstrates the wide pressure range over which a significant third harmonic can be generated by the use of multiple Bessel beams.

B. Three and more than three input Bessel beams

If one uses three ring slits in the front focal plane one has three Bessel beams interacting simultaneously with the nonlinear medium. The third-harmonic photon can now be formed also by the combination of one photon each from the three slits. This (1+1+1) combination of the photons of the fundamental is in addition to the (2+1) and (3+0) combinations encountered earlier in the two slit case. For the three slits case these three combinations add up to give ten independent values of the cone angle β of the output Bessel beam components. Consequently the harmonic radiation in the three slits case is a superposition of ten Bessel beams. We leave the presentation of their detailed calculations for future experimental papers.

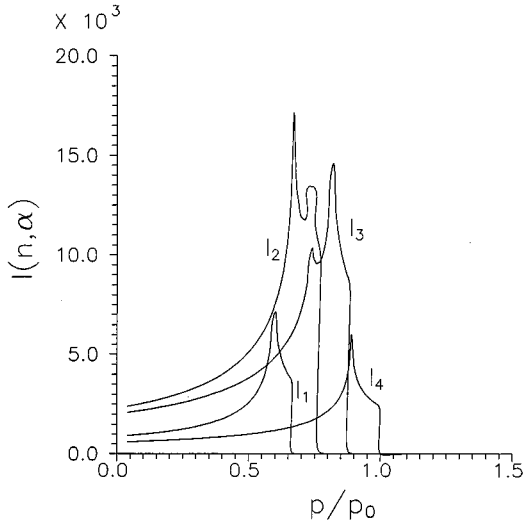

FIG. 2. The behavior of the four transverse-phase-matching integrals as functions of the pressure of the gas for a model system containing two Bessel beams in the input radiation are shown.

Note, however, that on increasing the number of slits from one to two, one encountered an increase in the tolerance width of the pressure (compare Fig. 3 (here) and Fig. 2 of Ref. [2]). Such an increase in the tolerance width does not occur in going from two to three slits if the third slit is introduced at an intermediate radius a_3 such that $a_1<a_3<a_2$. This is because the width of the curve in Fig. 3

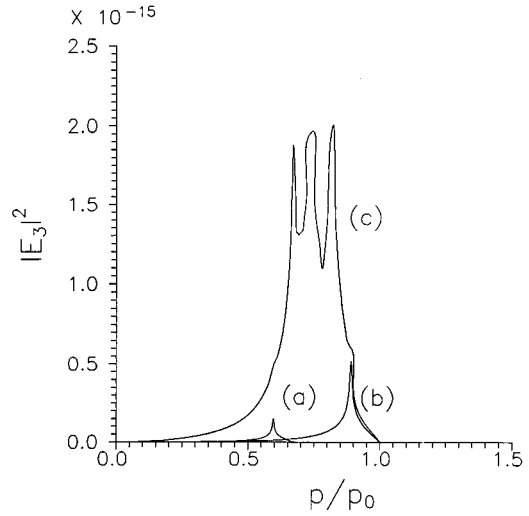

FIG. 3. The intensity of the third harmonic detected in the case of the two Bessel beams is plotted. Note the wide width of the curve when both Bessel beams are present.

is determined by the minimum and the maximum radii of the multiple ring slit system, and the overall interference effects of the superpositions of the multiple Bessel beams in the generated third harmonic. In the next section a model is discussed to obtain the radiation from a broad-ring slit.

C. The broad-ring slit

In the experiment of Ref. [1] a broad-ring slit was in use. One may represent a broad-ring slit comprising of a large number of thin-ring slits, lying side by side in the broad-annular region defined by an inner radius a and outer radius b. The field generated by such a broad-ring slit may be represented by an integral of the following type (see the Appendix)

$$\Psi_1^+ = A\int_a^b 2\pi r\,dr\,\exp\left(-ik\,\frac{f}{\mathcal{L}}\,z\right)J_0(\kappa r\rho/L), \quad (4.10)$$

$$A = \frac{\mathcal{A}}{i\lambda\bar{\mathcal{L}}}, \quad (4.11)$$

$$\mathcal{L}^2 = f^2 + r^2, \quad (4.12)$$

$$\rho^2 = x^2 + y^2, \quad (4.13)$$

$\bar{\mathcal{L}}$ is the average distance of the broad-ring aperture from the center of the lens; f is the focal length of the lens, λ is the wave length of the fundamental radiation, and $\mathcal{A}$ is a constant related to the amplitude of the radiation which illuminates the broad slit, and the geometry, as discussed briefly in the Appendix.

The generated third harmonic in the long-sample limit is then given by the expression similar to (4.2) where the function $\xi(z)$ is replaced by

$$\xi_c(z) = z\Bigg[(2\pi)^4\int_a^b r_1 dr_1\int_a^b r_2 dr_2\int_a^b r_3 dr_3\,\Xi(\beta) \times \delta\{k_3\cos\beta - \kappa f(\mathcal{L}_1^{-1}+\mathcal{L}_2^{-1}+\mathcal{L}_3^{-1})\} \times \int_0^\infty \rho\,d\rho\; J_0(k_3\rho\,\sin\beta)J_0(\kappa\rho r_1/\mathcal{L}_1) \times J_0(\kappa\rho r_2/\mathcal{L}_2)J_0(\kappa\rho r_3/\mathcal{L}_3)\Bigg]. \quad (4.14)$$

The difference between (4.14) and (4.2) is an additional effect. This is revealed by noting that in (4.14), there may be several combinations of slits with different radii, r_1, r_2, r_3 which simultaneously satisfy a longitudinal phase-matching condition corresponding to a particular β. Each one of these combinations has a different value of the transverse-phase-matching integral. Physically this additional effect to allow phase matching for a given value of β arises because the three photons can come not only from different azimuthal angles but also from several different values of the inclination to the z axis. The analytical evaluation of (4.14) has not been possible. We have numerically evaluated (4.14) by breaking the broad slit of Ref. [1] in to 11 slits lying in the annular region defined by $a=0.45$ cm, $b=0.55$ cm. Each slit is assumed to be of width 0.01 cm, and is placed with its center at the marker 0,1,2,3,4,5,6,7,8,9,10 separated by 0.01 cm. In this case there are as many as 286 values of β. In general for n slits one has $N[=n(n+1)(n+2)/6]$ distinct combinations of r_1, r_2, r_3 leading to the different values of β, some of which may be degenerate, depending on the value of the three radii. The intensity of the detected third harmonic is plotted in Fig. 3 of Ref. [2]. In Fig. 4 we accommodate the three cases viz. the single-slit, the two-slit, and the broad-slit (represented by 11-slit) configurations considered above. The unnormalized power detected at the end face of the sample of length 10 cm placed symmetrically in a region where the approximate Bessel beam is formed on the optical axis, is plotted in Fig. 4. For the sake of clarity each curve is multiplied by a suitable factor mentioned alongside each curve. The width of the broad-slit configuration is wider than that for a single-slit case but is narrower with respect to the two slit configuration. The reason for the reduction in the width is the effect of the intereference of the multiple Bessel beams of the TH produced in the broad-slit case. The intereference has much less detrimental effect for the two-slit configuration. The width is more but the power is much less in the two-slit case compared to the broad-slit case

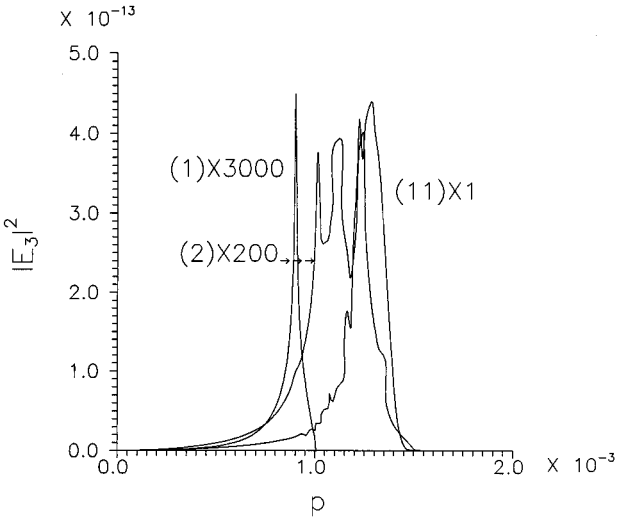

FIG. 4. Curves are the same as in Figs. 3 of Ref. [2] and those of Fig. 3 of this paper plotted with suitable multiplicative factors to be accommodated in the same graph. This is done to compare the various features of the curves. $a=0.45$, $b=0.55$, and $f=10.0$.

Lastly it is of interest to note the results of the present theory when the radii of the ring slit or the focal length of the lens is varied. By decreasing the radii and/or increasing the focal length one modifies the angle α to smaller values. This implies that the pressure of the gas at which the maximum THG may occur decreases. To demonstrate this we have plotted in Figs. 5 and 6 the three cases as in Fig. 4. Figure 5 shows the effect of increasing the focal length of the lens compared to that in Fig. 4; and Fig. 6 shows the effect of decreasing the radii of the annular slit with respect to those in Fig. 4. As mentioned above in both cases the pressures—at which the maximum occurs—decreases and the overall power is reduced. It remains to be seen if the experimental results would follow the same pattern.

In conclusion we have given besides the details of the

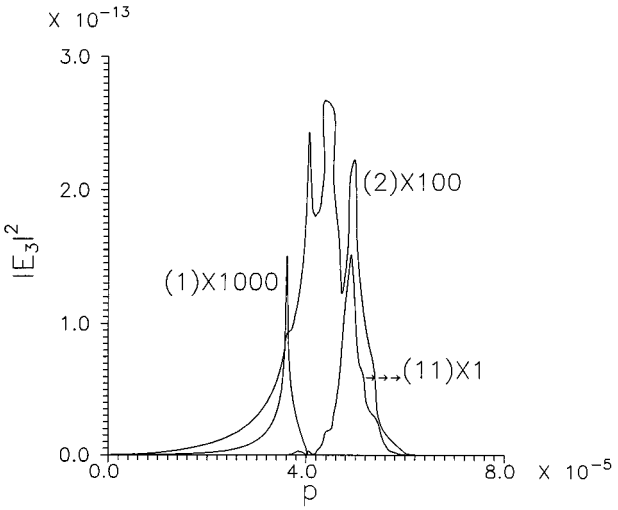

FIG. 5. Curves multiplied with indicated factors for the single-, double-, and 11-slit cases for the model (same as that in Fig. 4), but with $f=50.0$ are shown.

theory of the THG by Bessel beams an important result that the width of the pressure range can be controlled by controlling the radial distance between two-ring slits and filling the internal space either by a single-ring slit in between, or by a number of slits. There is much scope for improvement of the present formalism. For example, it is important to take into account the curvature of the wave front in the actual experiments of Ref. [1]. The curvature effects are expected to be important for shorter focal lengths where the THG is predicted to be higher by the present formalism.

ACKNOWLEDGMENTS

The visit of S.P.T. to Rochester was supported by the Indo-US project NSF.INT 9100 685. S.P.T. acknowledges the help of Ruchir Tewari in the computer calculations of the results discussed in IV C.

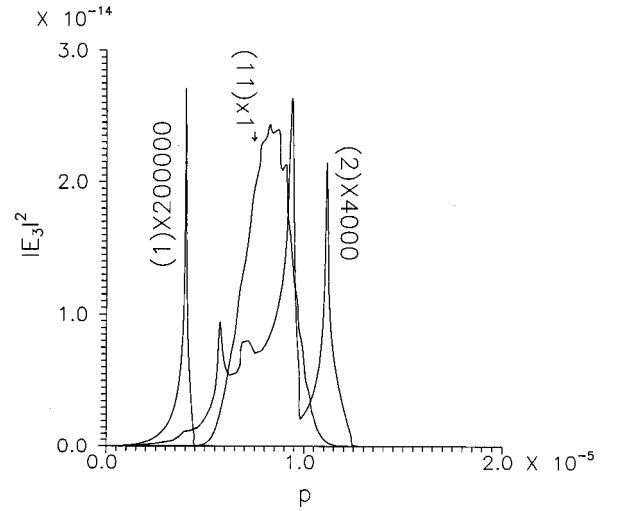

FIG. 6. Curves multiplied with indicated factors for the single-, double-, and 11-slit cases for the model $a=0.1$ cm, $b=0.15$ cm, $f=10.0$ cm, with an individual slit=0.005 cm are shown.

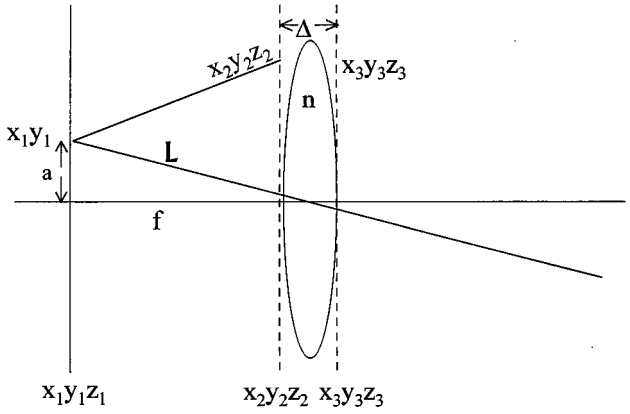

FIG. 7. The ring slit and lens arrangement used for producing a Bessel beam or a superposition of them is shown.

APPENDIX

The derivation of the Bessel function solution from a ring slit placed at the front focal plane of a convex lens is not new. It is included here for completeness and ready reference. Let the disturbance at the ring slit, in the plane $\Sigma_{x_1y_1}=(x_1,y_1,z=z_1)$ (see Fig. 7) be represented by

$$u(x_1,y_1,z_1)=\mathcal{A}\delta(x_1^2+y_1^2-a^2)\exp(-i\kappa z_1). \quad \text{(A1)}$$

The disturbance at the plane $\Sigma_{x_2y_2}=(x_2,y_2,z=z_1+f)$, just to the left of the lens, as shown in Fig. 7, is given by the scalar diffraction theory as

$$u(x_2,y_2,z_2)\int\int_{\Sigma x_1y_1}\frac{1}{i\lambda}\,u(x_1,y_1)\,\frac{\exp(i\kappa r_{21})}{r_{21}} \times\cos(\vec{n}\cdot\vec{r}_{21})\,dx_1dy_1. \quad \text{(A2)}$$

On using

$$(x_1,y_1)=a(\cos\phi,\sin\phi) \quad \text{(A3)}$$

$$\mathcal{L}^2=a^2+f^2,\quad \cos(\vec{n}\cdot\vec{r}_{21})\simeq 1 \quad \text{(A4)}$$

$$r_{21}^{(a)}\simeq\mathcal{L}\left[1+\frac{x_2^2+y_2^2}{2\mathcal{L}^2}-\frac{2a}{2\mathcal{L}^2}\{x_2\cos\phi+y_2\sin\phi\}\cdots\right] \quad \text{(A5)}$$

(A2) gives

$$u(x_2,y_2,z_2)=\frac{\exp(ik\mathcal{L})}{i\lambda\mathcal{L}}\int\int_{\Sigma x_1y_1}u(x_1,y_1)\,a\,da\,d\phi \times\exp\left[i\kappa\,\frac{x_2^2+y_2^2}{2\mathcal{L}}\right] \times\exp\left[-\frac{i\kappa a}{\mathcal{L}}\{x_2\cos\phi+y_2\sin\phi\}\right]. \quad \text{(A6)}$$

The disturbance on the plane $\Sigma_{x_3y_3}=(x_3,y_3,z=z_1+f+\Delta)$ to just right of the lens is given in the well-known manner by

replacing $x_2 \rightarrow x_3$, $y_2 \rightarrow y_3$ and introducing the modification of the curvature to the wave front due to the lens. We have

$$u(x_3,y_3,\mathcal{L}+\Delta)=\frac{\exp[i\kappa(\mathcal{L}+n\Delta)]}{i\lambda\mathcal{L}} \times \int\int_{\Sigma_{x_1y_1}} u(x_1,y_1)a\,da\,d\phi \times \exp\left[-i\kappa\frac{x_3^2+y_3^2}{2f}\right]\exp\left[-\frac{i\kappa a}{\mathcal{L}}\{x_3\cos\phi + y_3\sin\phi\}\right]\exp\left[i\kappa\frac{x_3^2+y_3^2}{2\mathcal{L}}\right]. \quad \text{(A7)}$$

Here Δ is the thickness of the lens and n is the refractive index of the material of the lens. The curvature of the wave front in the plane x_3,y_3 may be ignored as long as $(a/f)^2 \ll 1$. Let the disturbance to the right of the plane $z_3=\mathcal{L}+n\Delta$ be such a solution of the scalar wave equation which preserves the angular spectrum of the plane-wave solution, as represented by the disturbance on the x_3,y_3 plane, then in the region where the waves overlap one may write,

$$u(x,y,z)=\frac{\exp[i\kappa(\mathcal{L}+n\Delta)]}{i\lambda\mathcal{L}}\int\int_{\Sigma(a,\phi)}\mathcal{A}a\,da\,d\phi \times \exp\left(-i\kappa\frac{f}{\mathcal{L}}z\right) \times \exp\left[-i\frac{\kappa a}{\mathcal{L}}\{x\cos\phi + y\sin\phi\}\right]. \quad \text{(A8)}$$

This has been used as the incident fundamental Bessel beam in the text for small values of da and constant $\mathcal{A}$.

[1] B. Gluskho, B. Kryzhanovsky, and D. Sarkisyan, Phys. Rev. Lett. **71**, 243 (1993).

[2] Surya P. Tewari, H. Huang, and R. W. Boyd, Phys. Rev. A **51**, RC2707 (1995).

[3] J. Durnin, J. Opt. Soc. Am. A **4**, 651 (1987).

[4] J. Durnin, J. J. Miceli, Jr., and J. H. Eberly, Phys. Rev. Lett. **58**, 1499 (1987).

[5] See also P. W. Milloni and J. H. Eberly, *Lasers* (Wiley, New York, 1988), p. 524–529.

[6] For J_0-like beams with lenses, see, S. M. Herman and T. A. Wiggins, J. Opt. Soc. Am. A **8**, 932 (1991).

[7] W. Magnus and F. Oberhettinger, *Formeln Satze fur die Spiezziellen Funkitionen der Mathematischen Physik* (Springer, New York, 1948), Art. 1, Sec. 3; see also, G Arfken, *Mathematical Methods for Physicists*, 3rd ed. (Academic, New York, 1985), p. 594.